RSC Advances

ROYAL SOCIETY OF CHEMISTRY

www.rsc.org/advances

Journal Name RSC

COMMUNICATION

Encapsulation of Selenium in Porous Hollow Carbon Spheres for Advanced Lithium-Selenium Batteries

Yanqing Lai[a], Fuhua Yang[a], Zhian Zhang*[a], Shaofeng Jiang[a], and Jie Li[a]

Porous hollow carbon spheres (PHCSs) with high surface area and large pore volume were synthesised using a facile template method. After selenium (Se) encapsulation, Se/PHCS composite was formed. The obtained Se/PHCS composite was demonstrated as a suitable cathode material for lithium-selenium batteries.

Rechargeable lithium batteries, being used as the power source for electric vehicles and mobile devices, have been received great attention in recent years.[1] Among rechargeable lithium battery systems, lithium-sulfur (Li-S) batteries have attracted much more attention because of their high theoretical specific capacity (1672 mA h g^{-1}) and specific energy density (2600 W h kg^{-1}).[2,3] Though there are still many challenges on the road to a viable Li-S battery, the progresses achieved in the past decade have been significant.[4]

Selenium, belonging to the same group in the periodic table with sulfur, should be an attractive alternative cathode material for rechargeable lithium batteries for its similar chemical properties with sulfur. Compared with sulfur cathode, selenium cathode shows superior advantages.[5,6] Selenium have higher electric conductivity than sulfur (20 orders of magnitude higher than sulfur), suggesting that Se have higher utilization rate and faster electrochemical reaction with Li. Although the theoretical gravimetric capacity of the selenium (675 mAh g^{-1}) is lower than that of sulfur (1672 mAh g^{-1}), the theoretical volumetric capacity of selenium (3253 mA h cm^{-3}, based on the selenium density of 4.82 g cm^{-3}) is comparable to that of sulfur (3467 mAh cm^{-3} based on the sulfur density of 2.07 g cm^{-3}).[7] These advantages make selenium a prospective alternative cathode material for high energy density rechargeable lithium batteries. However, unlike Li-S batteries, researches on Li-Se batteries are still at a very early stage. Similar to Li-S batteries system, the selenium cathodes also face the dissolution issue of high-order polyselenides, resulting in fast capacity fading, poor cycle performance and low Coulombic efficiency.

In response to the above challenges, several strategies have been attempted in recent years.[6-13] Among all these efforts that have been made, preparing selenium/carbon (Se/C) composite seems to be an effective way, not only because the Se/C composites improve the electrical conductivity but also retard the shuttle effect by host the polyselenide in the matrix.[7~11,13] During the past years, attempts have been made to fabricate Se/C composites using carbon materials such as polyacrylonitrile (PAN) derived carbon[11] and carbon nanotubes (CNTs)[13]. Wu et al.[11] prepared the Se/C composite using a simple combination method of ball milling and low temperature treatment of Se/PAN mixture, the composite maintained a discharge capacity of 244 mAh g^{-1} after 10 cycles at the current density of 100 mA g^{-1}. Abouimrane et al.[13] showed that Se/CNT cathode can deliver a reversible capacity of more than 300 mAh g^{-1} at low current density C/12 (50 mA g^{-1}). Although improvements resulted, the cathodes still suffered from inadequately contact between the active material and the electronic conductors. To overcome the above shortage, porous-structured carbon materials with high surface area were tested and proved to be a promising cathode material. Wang et al.[8] impregnated Se into a porous-structured carbon sphere at a temperature of 600℃ under vacuum to form a Se/C composite with excellent electrochemical performance. The porous material effectively improves the selenium utilization and restrains the solubility of polyselenides on account of large surface area, abundant porous channels and strong adsorbent properties. However, the loading of active mass in the Se/C composites is low (30.0 wt.% Se) due to the limited pore volume (0.2 cm^3 g^{-1}). Here, we focus on the research of encapsulating Se into porous carbon materials with large pore volume to achieve high selenium content composite as cathode for Li-Se batteries.

Porous hollow carbon spheres (PHCSs) have been proved to be an promising matrix material.[14,15] With the unique properties of porous hollow-structured, high surface area and large pore volume, PHCSs will load more selenium, minimize the shuttle effect, preserve fast transport of lithium ions by ensuring good electrolyte penetration and facilitate good transport of electrons when used as Li-Se batteries electrode. However, encapsulating Se into PHCSs as cathode has rarely been reported yet.

Herein, we report a selenium/PHCS (Se/PHCS) composite with high Se content of 60.0 wt.% exhibits high reversible capacity and Coulombic efficiency. HCNSs were prepared by a simple template approach using silica and resorcinol/formaldehyde (RF) as template and carbon precursor respectively. By infusing Se into PHCSs at a temperature of 260 ℃, Selenium/HCNS (Se/HCNS) composite were synthesized. The Se/PHCS composite exhibits a reversible charge/discharge capacity 338 mAh g^{-1} after 50 cycles and high Coulombic efficiency (ca. 97.5%) at 0.1 C charge-discharge rate.

The mechanism for the formation of silica@RF spheres can be described as follow:[16-18] In the solution, containing ammonia, ethanol and deionized water, both the tetrathoxysilane (TEOS) and RF undergo hydrolysis reaction. For TEOS, its hydrolysis proceeds much faster (taking about 1 h), and silica spheres are generated firstly. Because of the negative charge on the silica spheres, NH_4^+ ions can cover its outer surface easily. While the reaction between resorcinol and formaldehyde catalyzed by OH^- always takes 24 h. Due to electrostatic attraction between the negative OH^- groups of RF polymer and positive NH_4^+ ions on the silica surface, a polymer layer form on the silica surface.

The SEM and TEM images of the PHCSs are shown in Fig. 1(a), (c). From the Fig. 1(a), it can be seen that the carbon sphere have a highly uniform spherical shape without any structural damage, the diameters of the HCNSs range from 100 nm to 200 nm. A typical TEM image shown in Fig. 1(c) reveals that the spheres have a hollow structure with large internal void space and thin shells. Fig. 1(b), (d), (e), (f) and (g) show the SEM, TEM, and Annular dark-field TEM image, and corresponding Se and C elemental mapping of Se/PHCS. After selenium impregnate in the pores of PHCSs, the morphology of the carbon spheres barely changed. The TEM image in Fig. 1(d) shows that the carbon-selenium composite also has a hollow structure. Notably, the shells of the Se/PHCS become darker than that of PHCSs in Fig. 1(c), a sign of selenium impregnation in the shell pores, similar phenomenon have been reported.[19] The elemental mapping on Se/HCNS in Fig. 1(e), (f), (g) reveals the presence and uniform distribution of selenium in Se/PHCS.

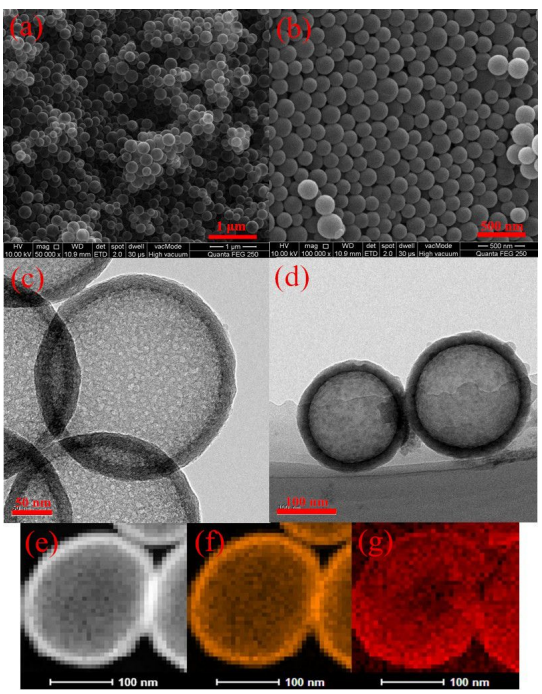

Fig. 1 SEM images of PHCS (a) and Se/PHCS (b), TEM images of PHCSs (c) and Se/PHCS (d), Annular dark-field TEM image (e), and corresponding Selenium (f) and Carbon (g) elemental mapping.

The nitrogen (N_2) adsorption-desorption isotherms and pore-size distribution curves of PHCSs and Se/PHCS composite are derived from BET measurements. As shown in Fig. 2(a), the curve of the PHCSs exhibit a type Ⅳ isotherm was observed, indicating the characteristic mesoporous structure of the PHCSs, these pores can act as pathways for the impregnation of selenium into the interior when the Se/C composite is formed. The adsorption-desorption hysteresis of PHCSs is larger than that of Se/PHCS, suggesting that PHCSs possesses larger volume of mesopores. This conclusion is supported by the pore size distribution curves of PHCSs and Se/PHCS (Fig. 2(b)). With the incorporation of Se into the PHCSs framework, the BET surface area, total pore volume are decreased to 31.5 m^2 g^{-1} and 0.10 cm^3 g^{-1} from the initial 859 m^2 g^{-1} and 1.24 cm^3 g^{-1} respectively, and the average pore diameter increases from 5.76 nm to 12.9 nm, indicting that the small pores are occupied by selenium nanoparticles.

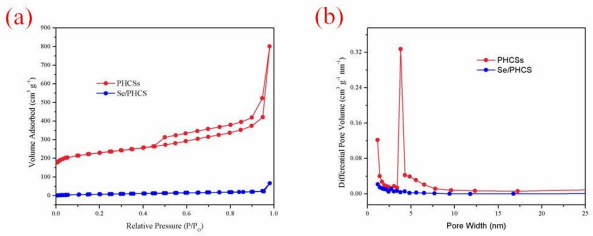

Fig. 2 Porosity characterization of PHCSs and Se/PHCS composite: N2 sorption isotherms(a), pore size distribution(b).

X-ray diffraction (XRD) patterns of elemental selenium (AR, Aladdin, China), PHCSs and the Se/PHCS are given in Fig. 3(a). For selenium, several peaks at 23.5° (100), 29.7° (101), 41.3° (110), 43.6° (102), 45.4° (111), 51.8° (201), 55.7° (112), and 61.5° (202) are in good accord with the diffraction peaks of selenium, which can be indexed to the trigonal phase of Se (JCPDS 06-0362).[20,21] The XRD patten of the PHCSs shows a broad reflection at 2θ of about 24°, which can be attributed to the amorphous characteristic of the as-prepared PHCSs.Fig. S1 shows the Raman spectra of the HCNSs. Two peaks are observed at 1345.9 and 1585.0 cm^{-1} ascribed to D-bang and G-band respectively. The intensity ratio (I_D/I_G) of the two bands is about 0.96, suggesting the partial graphitization degree of the as-obtained HCNSs. The Se/PHCS composite exhibits peaks perfectly matching with those of pure selenium, thus further indicating the presence of selenium in the Se/PHCS composite. To determine the selenium content in the Se/PHCS composite, thermogravimetric analysis (TGA) was carried out under a nitrogen atmosphere, as shown in Fig. 3(b). The TGA result shows that the selenium content is 60.0 wt% in the Se/PHCS composite.

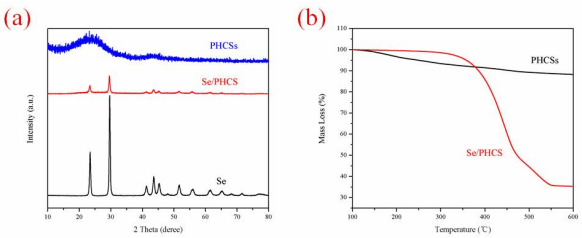

Fig. 3 XRD patterns of elemental selenium, PHCSs and Se/PHCS composite (a), TGA curve of the PHCSs and Se/PHCS composite (b).

A cyclic voltammogram (CV) of the Se/HCNS composite is shown in Fig. 4(a). The pair of sharp redox peaks indicates that

during charge/discharge the electrochemical reduction and oxidation of selenium occurs in two stages. The first peak at 2.2 V involves the reduction of elemental selenium to lithium polyselenide Li_2Se_n ($n \geqq 4$). The second peak at 1.75 V involves the reduction of selenium in lithium polyselenide to Li_2Se_2 and Li_2Se. Two oxidation peaks are observed at 1.9 V and 2.4 V. Notably, no obvious changes in the CV peak positions or peak current are observed in CV curves, confirming the electrochemical stability of the Se/HCNS composites and indicating that the porous carbon structure is quite effective in preventing the loss of selenium into the electrolyte and improving Coulombic efficiency with cycling.

The charge-discharge profiles within a cut-off voltage window of 1-3 V, as show in Fig. 4(b), are generally in agreement with the CV results. There exist two discharge plateaus, namely, 2.2 V and 1.8 V, be ascribed to the reduction of Se to Li_2Se_n ($n \geqq 4$) and Li_2Se_n ($n \geqq 4$) to Li_2Se_2 and Li_2Se respectively. This is consistent with the mechanism of Li-Se batteries that proposed in Abouimrane's previous research. The charge plateaus involve the oxidation of lithium polyselenide. The Se/PHCS composite cathode shows a discharge capacity of 590 mAh g^{-1} in the first cycle, and maintains 473 mAh g^{-1} in the 10th cycle.

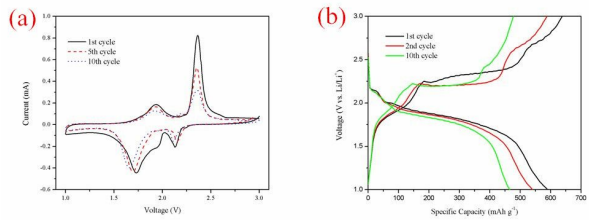

Fig. 4 Cyclic voltammograms of the Se/PHCS composite cathode at a scanning rate of 0.2 mV s^{-1} (a), and charge-discharge curves of the Se/HCNS at different cycles at a current density of 0.1 C (b).

Fig. 5(a) displays the cycling performance of Se/PHCS and pristine Se cathodes. At a constant current density of 0.1C, the initial discharge capacity of the Se/PHCS composite and pristine Se is 590 and 447 mAh g^{-1}, respectively. The Se/PHCS shows much better cycling stability with a reversible capacity of 338 mAh g^{-1} after 50 cycles. In contrast, the discharge capacity of pristine Se cathode dropped to 75 mAh g^{-1} (from 447mAh g^{-1}) by 50 cycles, which is less than 25% of the value for Se/PHCS. In addition, the columbic efficiency of Se/PHCS (ca. 97.5%) is higher than that of pristine Se.(Fig.5(b)) The excellent electrochemical performance of the Se/PHCS can be attributed to the characteristics of the carbon material (PHCSs). The porous hollow framework of the PHCSs not only confine selenium and minimize loss of lithium polyselenide, thus retard the shuttle effect, but also facilitate transport of Li^+ ions in the electrolyte. Moreover, the conductive character of the carbon framework allows good transport of electrons from/to the poorly conducting active material.

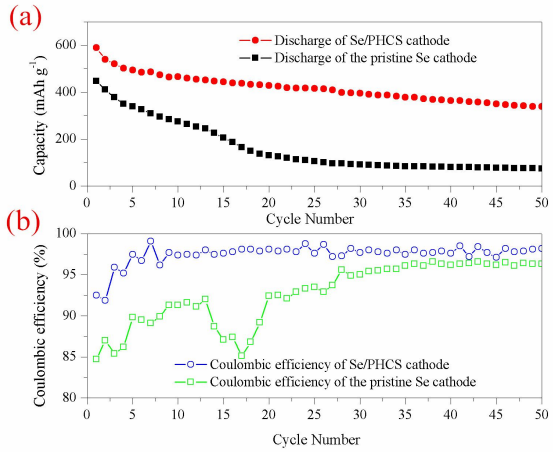

Fig. 5 Cycling performance(a) and coulombic efficiency(b) of the pristine Se and Se/PHCS composite cathodes at 0.1 C within a voltage range of 1-3V.

To get further insight into the improved electrochemical performance with the use of PHCSs, electrochemical impedance spectroscopy (EIS) analysis was carried out. Fig. 6 shows typical Nyquist plots of the Se/PHCS composite and pristine Se. The impedance plots are composed of a depressed semicircle at high frequency, and inclined line at low frequency. The diameter of the semicircle corresponds to the charge transfer resistance (R_{ct}) of the cell which is manly generated at the interface between the electrode and the electrolyte. It is obvious that the R_{ct} relating to the electrochemical activities of the Se/PHCS composite is significantly decreased compared with that of the pristine Se (decreases by about 30%). This can be evidently ascribed the electronic conductive network of PHCSs. The PHCSs matrices with a good electrical conductivity can serve as the conductive channels between elemental Se, which decreases the inner resistance of battery and is favorable for stabilizing the electronic and ionic conductivity, therefore leading to a higher specific capacity.

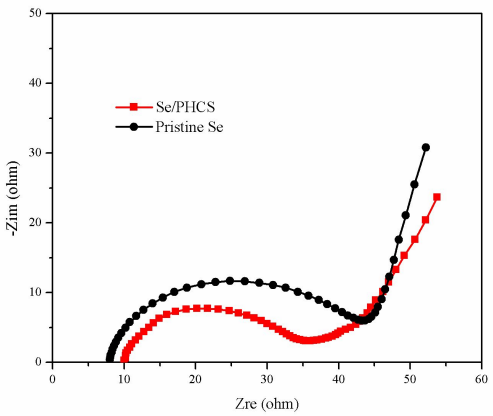

Fig. 6 Nyquist plots of the Se/HCNS and Pristine Se.

Conclusions

We have fabricated porous hollow carbon spheres with high surface area and large pore volume through a facile template method. The Se/PHCS composites with Se content of 60.0 wt.% were synthesized by a melt-diffusion strategy. The composites effectively improve the electronic conductivity, and

inhibit the dissolution of polyselenides, so the Li-Se batteries display a high electrochemical performance. The first discharge capacity of the Se/PHCS composite is 590 mAh g^{-1} at 0.1 C, which is 87.4% of the theoretical specific capacity. After 50 cycles, the capacity remains as high as 338 mAh g^{-1}, much higher than that of pristine Se cathode (only 75 mAh g^{-1} remain after 50 cycles). Moreover, the Se/PHCS maintain a high Coulombic efficiency (above 97%) after serval cycles. Consequently, the Se/PHCS composites with porous hollow structure have great potential for application in high-energy-density Li-Se batteries.

Notes and references

[a]*School of Metallurgy and Environment, Central South University, Changsha 410083, China. Fax: +86 731 88830649; Tel: +86 731 88830649; E-mail: zza75@163.com.*

† Electronic Supplementary Information (ESI) available: [Detailed Experimental and Raman spectra result]. See DOI: 10.1039/c000000x/

1 J. M. Tarascon and M. Armand, *Nature*, 2001, **414**, 359.
2 P. G. Bruce, S. A. Freunberger, L. J. Hardwick and J. M. Tarascon, *Nat. Mater*, 2012, **11**, 19.
3 Y. V. Mikhaylik and J. R. Akridge, *J. Electrochem. Soc*, 2004, **151**, A1969.
4 Y. Yang, G. Zheng and Y. Cui, *Chem. Soc. Rev*, 2013, **42**, 3018.
5 A. Abouimrane, D. Dambournet, K. W. Chapman, P. J. Chupas, W. Weng, and K. Amime, *J. Am. Chem. Soc*, 2012, **134**, 4505.
6 L. Liu, Y. Hou, S. Xiao, Z. Chang, Y. Yang, and Y. Wu, *Chem. Commun*, 2013, **49**, 11515.
7 C. P. Yang, S. Xin, Y. X. Yin, H. Ye, J. Zhang, and Y. G. Guo, *Angew. Chem. Int. Ed*, 2013, **52**, 8363.
8 C. Luo, Y. Xu, Y. Zhu, Y. Liu, S. Zheng, A. Langrock and C. Wang, *ACS nano*, 2013, **7**, 8003.
9 K. Han, Z. Liu, H. Ye and F. Dai, *J. Power Sources*, 2014, **263**, 85.
10 D. Kundu, F. Krumeich and R. Nesper, *J. Power Source*, 2013, **236**, 112.
11 L. Liu, Y. Hou, Y. Yang, M. Li, X. Wang and Y. Wu, *RSC Adv*, 2014, **4**, 9086.
12 Z. Zhang, X. Yang, X. Wang, Q. Li, and Z. Zhang, *Solid State Ionics*, 2014, **260**, 101.
13 Y. Cui, A. Abouimrane, C. J. Sun, Y. Ren, and K. Amine, *Chem Commun*, 2014, **50**, 5576.
14 N. Jayaprakash, J. Shen, S. S. Moganty, A. Corona and A. Archer, *Angew. Chem*, 2011, **123**, 6026.
15 C. Zhang, H. B. Wu, C. Yuan, Z. Guo and X. W. Lou, *Angew. Chem*, 2012, **124**, 9730.
16 A. B. Fuertes, P. Valle-Vigón and M. Sevilla, *Chem. Commun*, 2012, **48**, 6124.
17 A. H. Lu, G. P. Hao and Q. Sun, *Angew. Chem. Int. Ed*, 2011, **50**, 9023.
18 J. Liu, S. Z. Qiao, H. Liu, J. Chen, A. Orpe, D. Zhao and G. Q. Lu, *Angew. Chem. Int. Ed*, 2011, **50**, 5947.
19 G. He, S. Evers, X. Liang, M. Cuisinier, A. Garsuch and L. F. Nazar, *ACS nano*, 2013, **7**, 10920.
20 X. M. Li, Y. Li, S. Q. Li, W. W. Zhou, H. B. Chu, W. Chen, I. L. Li and Z. K. Tang, *Cryst. Growth Des*, 2005, **5**, 911.
21 B.Cheng, E.T. Samulski, *Chem. Commun*, 2003, **16**, 2024.
22 Y. Cui, A. Abouimrane, J. Lu, T. Bolin, Y. Ren, W. Weng, C. Sun, V. A. Maroni, S. M. Heald, and K. Amine, *J. Am. Chem. Soc*. 2013, **135**, 8047.

